Measurement 137 (2019) 168–178

Contents lists available at ScienceDirect

Measurement

journal homepage: www.elsevier.com/locate/measurement

Low-cost GNSS receiver in RTK positioning under the standard ISO-17123-8: A feasible option in geomatics

María S. Garrido-Carretero *, María C. de Lacy-Pérez de los Cobos, María J. Borque-Arancón, Antonio M. Ruiz-Armenteros, Rubén Moreno-Guerrero, Antonio J. Gil-Cruz

Departamento de Ingeniería Cartográfica, Geodésica y Fotogrametría/Centro de Estudios Avanzados en Ciencias de la Tierra, CEACTierra/Grupo de Investigación Microgeodesia Jaén, Universidad de Jaén, Campus Las Lagunillas s/n, Edif. A3, 23071 Jaén, Spain

ARTICLE INFO

Article history:
Received 13 September 2018
Received in revised form 11 January 2019
Accepted 15 January 2019
Available online 21 January 2019

Keywords:
GNSS
RTK positioning
ISO standards
Single-frequency GNSS receiver
Multi-frequency GNSS receiver

ABSTRACT

GNSS positioning is nowadays applied for surveying and other geomatic applications. Although dual-frequency GNSS receivers are widely used, low-cost single-frequency receivers have been relegated to navigation applications. However, their advantages make them optimum candidates for positioning applications in many scientific areas. To know the precision limits of these measuring systems, the evaluation of the uncertainty of measurement results obtained by them is required. For that, it is recommended to apply standard operating procedures (SOP). The International Organization for Standardization (ISO) published the standard ISO 17123-8 aimed at specifying field procedures to be adopted when determining and evaluating the precision of GNSS field measuring systems in real-time kinematic (RTK). Using this standard, we evaluate the positioning performance of two GNSS receivers, the geodetic dual-frequency Leica GS10 with AS10 antenna using a network RTK solution, and the low-cost single-frequency u-blox NEO-M8P using a single-base RTK solution. Considering the different sources of uncertainty and their influence quantities, the combined uncertainty budget for the dual-frequency receiver gives combined standard uncertainties on the horizontal position at the order of ±2.5 mm and close to ±4.5 mm for the vertical coordinate. In the case of the low-cost receiver, the combined standard uncertainties are close to ±5.5 mm for the horizontal position and ±11 mm for heights. The results indicate that just as the geodetic receiver satisfies the horizontal and vertical sub-centimetric precision limits established for high precision applications, the low-cost receiver can achieve a competitive positioning performance to survey-grade receivers in real-time positioning for short baselines.

1. Introduction

Global Navigation Satellite Systems (GNSS) are nowadays widely applied in surveying and other geomatic applications, especially using RTK positioning. This technique is usually performed using high precision GNSS receivers in order to achieve high precision and accurate results although, in recent times, there is a growing interest in the use of low-cost receivers. Thus, in 2008, [1] carried out some field tests to evaluate the GPS-RTK performance with low-cost single-frequency antenna and receivers concluding that it is feasible to apply consumer-grade antenna and receiver to GPS-RTK and that there is a small difference between the consumer-grade and the geodetic-grade receivers. However, to improve the performance, they recommended the use of a geodetic-grade antenna. Recent studies show that low-cost single-frequency RTK receivers can achieve competitive ambiguity resolution and positioning performance to survey-grade high-cost dual-frequency receivers: making use of low-cost single-frequency dual GNSS system (SF-DS) receivers and patch antennas [2], combining low-cost receivers with survey-grade antennas [3] or even in RTK positioning with a smartphone implementation of a single-frequency receiver for different ionospheric disturbance periods [4]. The performance of the Network Real Time Kinematic (NTRK) approach using a low-cost RTK board for Arduino environment, a smartphone with open source application for Android and the availability of data correction from a CORS service is analyzed in [5]. Other studies on single-frequency RTK using low-cost GNSS receivers can be found in [6,7].

It is known that the main limitation of traditional RTK positioning based on a single reference station is caused by distance-dependent errors (orbital errors and ionospheric and tropospheric

* Corresponding author.
E-mail address: mgarrido@ujaen.es (M.S. Garrido-Carretero).

https://doi.org/10.1016/j.measurement.2019.01.045
0263-2241/

refraction), being limited to a few kilometers [8]. Nevertheless, these errors can be modeled using GNSS observations from several reference stations around the rover position, extending the single-base RTK positioning to a multiple reference station solution or Network-based Real-Time Kinematic (NRTK). Different approaches coexist to generate the NRTK corrections, including MAX and i-MAX- Individualized MAX-solutions based on the MAC approach, Pseudo-reference Station (PRS), FKP (Flächen Korrektur Parameter) and VRS (Virtual Reference Station). For a detailed description about these techniques, reader is refereed to [9]. The most widely used are Master Auxiliary Concept (MAC) [10] and Virtual Reference Station (VRS) [11]. In the MAC approach, network corrections are calculated considering a main reference station or master (it is the nearest reference station to the rover location) and several auxiliary reference stations. This approach was designed to transmit network corrections in standard format under Networked Transport of RTCM via Internet Protocol (NTRIP) in a compact form [12], providing ambiguity-level observation data as correction differences of dispersive (ionospheric delay) and non-dispersive data (tropospheric delay and orbit errors) for each satellite-receiver pair. The main task of the network processing software considering the MAC approach is to reduce the ambiguities for the phase ranges from all reference stations in the network or sub-network to a common level. For ambiguity resolution, the software uses the known LAMBDA method [13]. The VRS approach also requires several reference stations connected to a network server. The rover sends a navigation solution of its current position to the network control center which accepts this position as the location of a virtual reference station, calculates the corrections relating to the VRS, and transmits them to the rover. As [14] shows, although from the user perspective both VRS and MAC approaches are supported by the main GNSS instruments and deliver positioning results at the same accuracy-level, the MAC approach appears to be superior, since it supplies raw correction data related to real reference stations, rather than modeled data related to virtual reference stations. Today, it is generally recognized that a RTK network or active network, comprised of permanent Continuously Operating Reference Stations (CORS), is an indispensable complement to GNSS positioning systems, allowing the determination of 3D positions in real-time with high precision and accuracy, and providing the fundamental infrastructure required to meet the needs of many surveying and mapping professionals, and navigation users.

All measuring processes are influenced by random and systematic errors. The evaluation of the precision and accuracy of a measuring system, including GNSS surveying, in order to achieve results that meet the quality specifications of a given project is a critical task. Several studies have been carried out to evaluate the precision and accuracy using NRTK solutions in Great Britain [15], Australia [16], Ireland [17], Taiwan [18], Spain [19], or Turkey [20], to name a few. Although the application of SOP for evaluating the uncertainty of measurement results of surveying instruments is not new, the complexity of the measuring GNSS systems complicated the introduction of testing methods for this kind of instruments. For that, the standard ISO 17123–8 for GNSS field measurement systems in RTK was introduced in 2007 and updated in 2015 [21,22]. [23] already revealed that some measuring ambiguities remain when applying this test procedure. Nowadays this is especially true when NRTK positioning is considered. Applications based on this official ISO standard considering NRTK solution are scarce. [24] evaluated the positioning performance of a low-cost high-sensitivity carrier phase-based navigation receiver based on the ISO standard for RTK geodetic receivers demonstrating its suitability for different accuracy levels of RTK positioning applications. In light of the developments with low-cost receivers, [25] evaluated two low-cost high sensitivity receivers in control surveying specifications using static GNSS positioning. The evaluation was carried out within a framework of published standards and guidelines. More recently, [26] proposed a methodology that combines both check and calibration procedures of a single GNSS receiver using the VRS method constituting a supplement to the standard ISO 17123-8.

In this study, the standard ISO 17123-8 is applied in order to evaluate the RTK performance of two GNSS receivers, the geodetic dual-frequency Leica GS10 with AS10 antenna considering network-based RTK solution, and the low-cost single-frequency u-blox NEO-M8P using a single-base station RTK solution. This manuscript is organized in five sections. In addition to this introduction, in Section 2, a brief description of the ISO standard is given. In Section 3 (data acquisition), the GNSS receivers as well as the field test procedures used are described. Section 4 shows the results and their statistical analysis, presenting the conclusions in Section 5.

2. ISO 17123-8 field procedures

The standard ISO 17123-8 [21] specifies field procedures to be adopted when determining and evaluating the precision (repeatability) of GNSS field measurement systems (from any constellation) in relative kinematic (GNSS RTK). Many times a number of effects are not perfectly accounted by the double-difference phase observations mathematical model. These effects enter as systematic factors in the observation noise, which is however modelled as pure random noise [27]. Therefore, since the adjustment GNSS (phase) observation model may be not completely correct. The covariance of GNSS baselines is often underestimated with respect their precision [28]. This is the reason why the repeatability is commonly used as a measure of the precision of the estimated coordinates by GNSS. The last edition includes the network RTK application and the calculation of an uncertainty budget [22]. Two different field procedures, namely simplified test procedure and full test procedure, are described. These tests are intended to be field verifications of the suitability of a particular instrument for a specific application, and/or to satisfy the requirements of other standards. The full test procedure is designed for determining the experimental standard deviation for a single position and height measurement and it is adopted to determine the best achievable measure of precision of the equipment in use. Further, this full test procedure may be used to determine the measure of the precision of the equipment under given conditions, the measure of the precision of the equipment used in different periods of time or under different conditions (multiple samples), and the measure of the capability of comparison between different precision of equipment achievable under similar conditions. In this work, we selected the full test procedure applied to the two mentioned receivers under two different scenarios: case (a) for the dual-frequency receiver using network MAC corrections and case (b) for the low-cost single-frequency receiver using a single-base (reference) RTK solution (Fig. 1).

The procedure requires the measurement of two samples of thirty data each one (fifteen from R1 and fifteen from R2). A sample is composed of three series of measurements, each one separately by at least 90 min. Thus, multiple series of measurements tend to reflect influences such as variations in the ionospheric and tropospheric conditions and changes in satellite configuration. A series of measurements consists of five sets. Each set of measurements comprises successive measurement at two rover points R1 and R2. The time lag between successive sets is recommended to be approximately 5 min. In such a way, the span of a series of measurements is about 25 min, making the measurements to cover the variation cycle of a typical multipath influence which is estimated about 20 min.

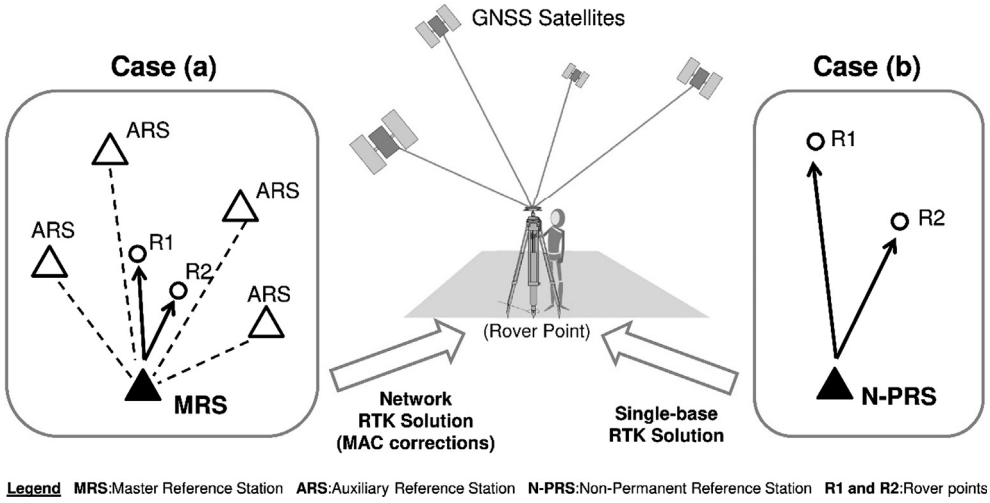

Fig. 1. Network configuration and differential RTK corrections applied in cases (a) and (b). Details of reference stations (MRS and N-PRS) are shown in Fig. 3.

For each set of points in a series, the horizontal distance (D) and height difference (Δh) between them is computed and compared to nominal values determined by methods with precision better than 3 mm other than RTK (see Section 3.C). Applying a least squares adjustment on overall measurements in all series, the estimates of x, y, and h for each rover point, their residuals for all measurements in the three series, and the experimental standard deviations of a single measurement of x, y, and h ($u_{ISO\text{-}GNSS\ RTK\text{-}xy} = s_{xy}$ and $u_{ISO\text{-}GNSS\ RTK\text{-}h} = s_h$, respectively) are calculated. In addition, the full test procedure allows us to perform statistical hypothesis tests to know if the calculated experimental standard deviations s_{xy} and s_h of a single position (x, y) and h are smaller than or equal to the corresponding value σ_{xy} and σ_h stated by the manufacturer or another predetermined value. Similarly, it can be tested if two experimental standard deviations of a single position (x,y) ($s_{xy(A)}$ and $s_{xy(B)}$) or h ($s_{h(A)}$ and $s_{h(B)}$) as determined from two different samples of measurements A and B belong to the same population.

3. Data acquisition

3.1. GNSS receivers

Different GNSS receivers were used in cases (a) and (b). The GNSS equipment used in case (a) is composed of a dual-frequency Leica GS10 receiver (equipment number 3660839), a triple frequency (GPS/GLONASS/Galileo) Leica AS10 antenna, and a radio field controller CS10 (Leica Geosystems AG. Heerbrugg, Switzerland) (Fig. 2a). The receiver is equipped with the Siemens MC75 GSM/GPRS module and was configured to receive NRTK corrections (MAC approach) from the Andalusian positioning network (RAP) (see Section 3.B) in RTCM format [29] via Internet Protocol (NTRIP). The RTK configuration and setting were 1-second observation rate, maximum PDOP = 6 and measurements number = 1, horizontal coordinate quality (CQ2D) ≤ 30 mm and vertical coordinate quality (CQ1D) ≤ 50 mm. The independence between ambiguity resolutions was guaranteed disconnecting to the RAP NTRIP caster between each two consecutive NRTK measurements. The standard deviations indicated by the manufacturer specifications considering the NRTK solution are $\sigma_{xy} = \pm(8\text{ mm} + 0.5\text{ ppm})$ for horizontal components and $\sigma_h = \pm(15\text{ mm} + 0.5\text{ ppm})$ for vertical component. In the case of single-base RTK positioning, the standard deviations are $\sigma_{xy} = \pm(8\text{ mm} + 1\text{ ppm})$ and $\sigma_h = \pm(15\text{ mm} + 1\text{ ppm})$ [30]. The height of the antenna was measured using the height hook with integrated tape measurement supplied with the instrument.

The GNSS receiver for the case (b) considers the low-cost single-frequency u-blox NEO-M8P GNSS RTK module (type number C94-M8P-3-11) (u-blox AG. Thalwil, Switzerland) (Fig. 2b and 2c). u-blox M8P modules use GPS L1 C/A, GLONASS L1OF, and BeiDou B1 observables. It is important to use a patch antenna with 10 cm diameter metallic ground plane in order to mitigate the multipath effect [31]. The base station module sends corrections using RTCM protocol to the rover module via a radio communication link enabling the rover to output its position relative to the base station down to centimeter-level precision. The manufacturer specifies the circular probable error (CEP) for RTK positioning as ±(25 mm + 1 ppm) (ppm limited to baselines up to 10 km). The convergence time is less than 60 s but it depends on atmospheric conditions, baseline length, GNSS antenna, multipath conditions, and satellite visibility and geometry [32]. The height of the antenna was reliably determined using together two accessories, the Leica GHM007 instrument height meter and GHT196 spacing bracket.

3.2. Configuration of the field test networks

According to the ISO standard procedure, the field tests include the base station and the two rover points previously mentioned. The separation D of rover points (Fig. 3a) shall be a minimum of 2 m and shall not exceed 20 m. In this work, the rover points R1 and R2 are located at the terrace of the Science and Technology building on the Campus of the University of Jaén (Spain) and are materialized by leveling benchmarks (Fig. 3b) belonging to a vertical control network deployed in the campus. We selected these points as they have a sky view free from obstacles. The horizontal distance (D) and height difference (Δh) between the rover points shall be determined by methods with precision better than 3 mm other than RTK. In our case we used a total station for the electronic distance measurement of D and high precision leveling for Δh (see Section 3.3). These values are considered as nominal values and are used in the first step of the full test procedure to ensure that RTK measurements are free from any gross error. This study considers two different RTK solutions, network-based in case (a) and single-base station in case (b). The reference stations and therefore the field tests are different in both cases.

In case (a), the network-based solution considers as reference frame the Andalusian Positioning Network [33]. This active GNSS network is a local geodetic infrastructure managed by the Institute

Fig. 2. Different instruments used in data acquisition: (a) Leica GS10 receiver and AS10 antenna on a surveying tripod, (b) u-Blox NEO-M8P GNSS antenna on a surveying tripod centered over the leveling benchmark and (c) Details of the NEO-M8P GNSS module and patch antenna.

Fig. 3. (a) Rover points R1 and R2 on the terrace of the Science and Technology building on the Campus of the University of Jaén (Spain) and the separation between them (D). (b) Detail of the benchmark for R1 and R2. (c) Location of reference stations (UJAE and UJAC) and the two rover points R1 and R2. (Background: orthoimage PNOA – Spanish National Plan of Aerial Orthophotgraphy). (d) Permanent reference station UJAE belonging to RAP active network on the terrace of the Hall of Residence Domingo Savio (Campus of the University of Jaén). (e) Non-permanent reference station UJAC on the terrace of the Hall of Residence Domingo Savio with u-Blox NEO-M8P GNSS module. (f) Leica AS10 antenna on reference station UJAC.

of Statistics and Cartography of Andalusia (IECA) for precise positioning applications in the Andalusian Community (South of Spain) [34]. The RAP network provides both NRTK corrections and GNSS data for accurate positioning through 22 permanent reference stations strategically distributed over the region of Andalusia with a maximum inter-stations distance of 70 km. The RAP permanent reference station UJAE (master reference station MRS considered in the network solutions, Fig. 1) is located at the campus on the terrace of the Hall of Residence Domingo Savio, at a distance of 335 m from R1 (Fig. 3c and 3d). On the other hand, for the case (b), the field test includes the non-permanent single-base (reference) station UJAC (Fig. 1), located at the same building than UJAE at a distance of 305 m from R1 (Fig. 3c and 3e). In the single-base RTK solution, the rover calculates its position relative to the location of this reference station UJAC. To get an optimal positioning accuracy, the accuracy of the reference station position must be guaranteed. For that, we previously carried out 3 h of static GNSS measurements at UJAC using the dual-frequency Leica GS10 receiver and AS10 antenna (Fig. 3f) with subsequent relative post-processing to obtain its coordinates in the same reference system and frame than the RAP network (ETRS89-ETRF2005).

For each network configuration, two independent samples A and B of thirty measurements each one were measured. The measurements were performed in 2018, on 31 January and 2 February (DOYs 031 and 033) for samples A and B in the case (a), and on 21 February and 7 March (DOYs 052 and 066) for samples A and B respectively in the case (b). All the collected data were referred to the ETRS89 - UTM projection (Zone 30) (x,y) considering the ellipsoidal height (h).

3.3. Determination of nominal values

The horizontal distance (D) between the two rover points was determined using a Leica TCA2003 total station (Fig. 4a). First, we checked that the difference between two independent horizontal distances R1-R2 and R2-R1 or closure error, equals to 0.1 mm, was acceptable using a 3σ tolerance (Eq. (1)).

$$T_{\Delta D} = \pm 3\sigma_D\sqrt{2} \tag{1}$$

where

$$\sigma_D = \pm\sqrt{(\sin V \cdot \sigma_{S_d})^2 + (S_d \cdot \cos V \cdot \sigma_V)^2} \tag{2}$$

$$\sigma_{S_d} = \pm\sqrt{\left(\frac{\sigma_{EDM}}{\sqrt{2}}\right)^2 + \sigma_i^2 + \sigma_r^2} \tag{3}$$

For each measurement, double face observations were performed on vertical angles (V) and slope distances (S_d). In Eqs. (2) and (3), the following source of uncertainty were considered: $\sigma_{EDM} = \pm(1\text{ mm} + 1\text{ ppm})$ for spatial distances, $\sigma_{V=}\sigma_{ISO\text{-}V} = \pm 1.5^{cc}$ for vertical angles, and instrument and reflector miscentering using optical plummet $\sigma_i = \sigma_r = \pm 0.001$ m. Then, we computed the arithmetic mean of both independent horizontal distances R1-R2 and R2-R1 (D), resulting as 16.1024 m. This distance is reduced to the UTM plane and then used as nominal distance for the identification of gross error. Propagating uncertainties, the standard uncertainty for D resulted as $\sigma_D/\sqrt{2} = \pm 0.0011$m. It is important to underline that the two slope distances measured using the classical double face approach may be correlated with each other, given the almost immediate sequence of observations and therefore very similar atmospheric conditions. Nevertheless, the numerical difference in Eq. (3) between considering or not the slope distances as independent variables is negligible and the obtained standard uncertainty is largely lower than the required precision of 3 mm.

On the other hand, the height difference (Δh) between the two rover points was measured by high precision leveling using a Leica DNA03 digital level and two bar code invar rods (Fig. 4b). Median mode was used and several observations were carried out for each measurement to the rod. The survey field procedure was applied according to the well-known rules of precise leveling [35]: (a) checking and adjusting level and rods before each survey, calculating the collimation error (digital level automatically corrects all the measurements); (b) correcting for the Earth's curvature; (c) starting and finishing each leveling run always with the same rod in order to avoid zero-point differences between rods; (d) double run between consecutive benchmarks; (e) lines of sight (between rods) less than 50 m. Balancing backsight and foresight distances in order to the total difference throughout the line is less than 10 cm. Equal number of setup for forward and backward runs; (f) double readings for backsight and foresight measurements keeping the time interval between readings as short as possible. The leveling method used was backsight-foresight-foresight-backsight (BFFB); (g) to prevent atmospheric refraction errors, the line of sight must not be below the first 50 cm of rod; and (h) avoiding windy conditions and excessive temperature changes during the measurements. We checked the discrepancy between the forward and backward height differences or misclosure error equals to 0.03 mm, establishing a 3σ tolerance for its acceptance. This tolerance (Eq. (4)), equals to ±0.23 mm, was computed based on the $\sigma_{ISO\text{-}LEV}$ standard uncertainty for the leveling equipment and the length of the leveled run (forward and backward distances) in km (K). According to [36], the experimental standard deviation

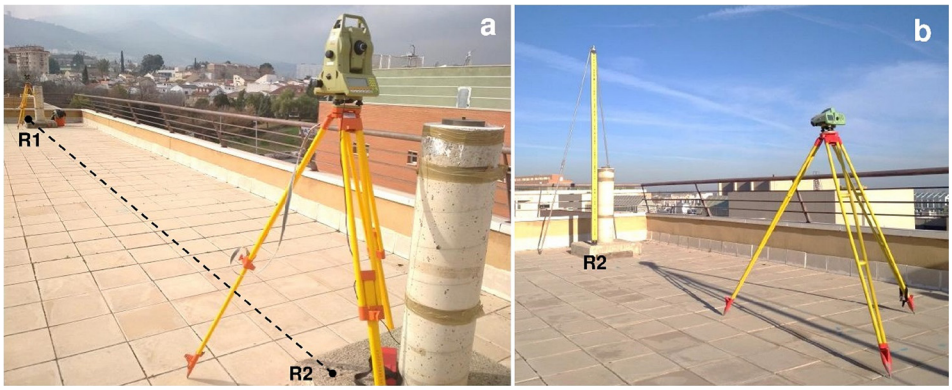

Fig. 4. Measuring the nominal values, horizontal distance (D) and height difference (Δh), between rover points R1 and R2 by using (a) Leica TCA2003 total station and (b) high precision leveling with a Leica DNA03 digital level and invar rods.

($\sigma_{ISO\text{-}LEV}$) of a 1-km double-run leveling for Leica DNA03 digital level with invar rods is ±0.3 mm.

$$T = \pm 3\sigma_{ISO-LEV}\sqrt{2}\sqrt{K} \quad (4)$$

Then, for the height difference Δh, we evaluated the mean of both forward and backward leveling runs Δh = −0.0153 m and its standard uncertainty $\sigma_{\Delta h}$ =±0.0004 m (Eq. (5)), K being the length of the forward or backward run, in km.

$$\sigma_{\Delta h} = \pm\sigma_{ISO-LEV}\sqrt{K} \quad (5)$$

4. Results

In total, 120 3D positions (x, y, and h) were measured corresponding to two samples (A and B) and two solutions (NRTK and single-base RTK). For each sample, fifteen positions (series S1, S2, and S3) were measured at each rover point. In Fig. 5, horizontal and vertical residuals from the network-based (top) and single-base (bottom) samples at rover points R1 and R2 are shown. The coordinates obtained by different series are very close to each other and there are no significant differences among the final values computed from different samples. As can be seen, considering the NRTK solution (dual-frequency receiver) at both rover points, the residuals are less than 5 mm in the north and east components and slightly higher in the vertical component. If single-base solution is considered (low-cost single-frequency receiver), the residuals double the values for the north and east components obtained with the NRTK solution and triple them for the vertical component. It should be noted that for high accuracy applications, the antenna calibration and its phase center variations (PCV) are needed. Available PCVs from International GNSS Service include corrections for geodetic antennas; however, antenna calibration is not available for low-cost antenna. [37] presents an approach to estimate the antenna phase centre offset (PCO) and variations (PCV) for an u-blox single-frequency patch antenna, based on relative calibration to a geodetic type antenna on a short baseline, considering two measurement sessions. The results clearly prove the impact of the phase center error on positioning accuracy, especially important in the vertical component. Therefore, it is important to underline that the unmodelled antenna correction could include a bias in the altimetric precision.

Initially, the calculation of the horizontal distance and height difference between the two rover points from the positions obtained in real-time is required. These measurements are compared directly with the nominal values in order to detect any measurement with gross error. No gross errors were detected in the two samples considered in cases (a) and (b). For each sample, and applying the least squares adjustment on overall measurements in all series, we estimated the average value of x, y, and h over the series, the summation of the squared residuals, the degrees of freedom for x, y, and h (they are identical for the three components), the experimental standard deviation for each component, and the standard deviation of a single measurement of x, y (s_{xy}) and h (s_h). Note that the ISO standard overestimates s_{xy} as it is computed as the mean square positional uncertainty. The probability represented by this circular precision index is in the range from 63% to 77%. Due to the variation in probability, this index is not recommended for using as a precision index because the probability represented varies when s_x and s_y are not equal. The preferred circular precision index, consistent with indexes used in the linear distribution, is the circular standard uncertainty, computed as the average of s_x and s_y [38]. The probability of the circular standard uncertainty is 39%, corresponding to the probability of the standard uncertainty ellipse. Therefore, the ellipse is commonly replaced by this circular form which is easier to use. Herewith, in this study, the circular standard uncertainty is used as the standard uncertainty of a single position ($u_{ISO\text{-}GNSS\ RTK\text{-}xy} = s_{xy}$). In addition, s_h is defined as the standard uncertainty of a single height ($u_{ISO\text{-}GNSS\ RTK\text{-}h} = s_h$). All these values are showed in Table 1. The standard uncertainty in a single position and in a single height for case (a) shows high similarity in both samples A and B ($s_{xy(A)}$ = ±1.6 mm and $s_{xy(B)}$ = ±1.8 mm, and $s_{h(A)}$ = ±3.3 mm and $s_{h(B)}$ = ±4.1 mm). The same trend is observed in case (b) ($s_{xy(A)}$ = ±3.3 mm and $s_{xy(B)}$ = ±3.5 mm, and $s_{h(A)}$ = ±9.7 mm and $s_{h(B)}$ = ±9.3 mm). As expected, vertical standard uncertainties have larger values compared to the horizontal ones, but they are still satisfactory in both cases. The values of the standard uncertainties on the horizontal positions s_{xy} considering the single-base RTK solution double the values for the NRTK solution and triple them again for the height components s_h.

Regarding the statistical hypothesis tests described in the ISO standard for the full test procedure (Section 2), the following four null hypotheses can be tested:

Ho_1) The calculated experimental standard deviation s_{xy} of a single position (x, y) is smaller or equal to a corresponding value stated by the manufacturer σ_{xy} or another predetermined value.

Ho_2) The calculated experimental standard deviation s_h of a single height h is smaller or equal to a corresponding value stated by the manufacturer σ_h or another predetermined value.

Ho_3) Two experimental standard deviations $s_{xy(A)}$ and $s_{xy(B)}$ of a single position (x, y) determined from two different samples of measurement belong to the same population, assuming that both samples have the same number of degrees of freedom.

Ho_4) Two experimental standard deviations $s_{h(A)}$ and $s_{h(B)}$ of a single height h, determined from two different samples of measurement, belong to the same population, assuming that both samples have the same number of degrees of freedom.

The experimental standard deviations $s_{xy(A)}$ and $s_{xy(B)}$ (or $s_{h(A)}$ and $s_{h(B)}$) may be obtained from two samples of measurement by the same equipment or from two samples of measurement by different equipment. In this study, the first option has been applied.

For null hypotheses Ho_1 and Ho_2, the calculated experimental standard deviations s_{xy} and s_h are compared to predetermined values σ_{xy} and σ_h using the χ^2 distribution [22,39] at the 95% confidence level with 56 and 28 degrees of freedom respectively. For case (a), the predetermined standard deviations as derived from the manufacturer specifications are σ_{xy} = ±8 mm and σ_h = ±15 - mm, and $\sigma_{xy} = \sigma_h$ = ±21 mm for case (b). For the low-cost single-frequency receiver, the manufacturer indicates only CEP in the product specifications [32] as term associated with GPS uncertainty. The CEP probability is 50%, hence the following conversion factor is used to determine the circular standard deviation σ = ±CEP/1,1774 for the normal circular distribution [38]. Although CEP is an index for the horizontal uncertainty only, and typically the vertical uncertainty is 2 to 3 times worse than the horizontal one, this index will be considered for the vertical component as well as no other uncertainty index is specified by the manufacturer for this component. Regarding null hypotheses Ho_3 and Ho_4, the standard deviations $s_{xy(A)}$ and $s_{xy(B)}$ (and $s_{h(A)}$ and $s_{h(B)}$) for both samples are tested using the F distribution at the 95% confidence level [22,40], verifying that the data measured in different days belong to the same population. As shown in Table 2, all four null hypotheses are accepted.

4.1. Combined standard uncertainty evaluation

The sources of uncertainty and their influence quantities are summarized in Table 3 for the NRTK solution (case a) and in Table 4 for the single-base RTK solution (case b). It should be noted that the uncertainty related to the sensitivity of the tubular/circular level can be neglectable using a tripod or pillar [41,42]. Related

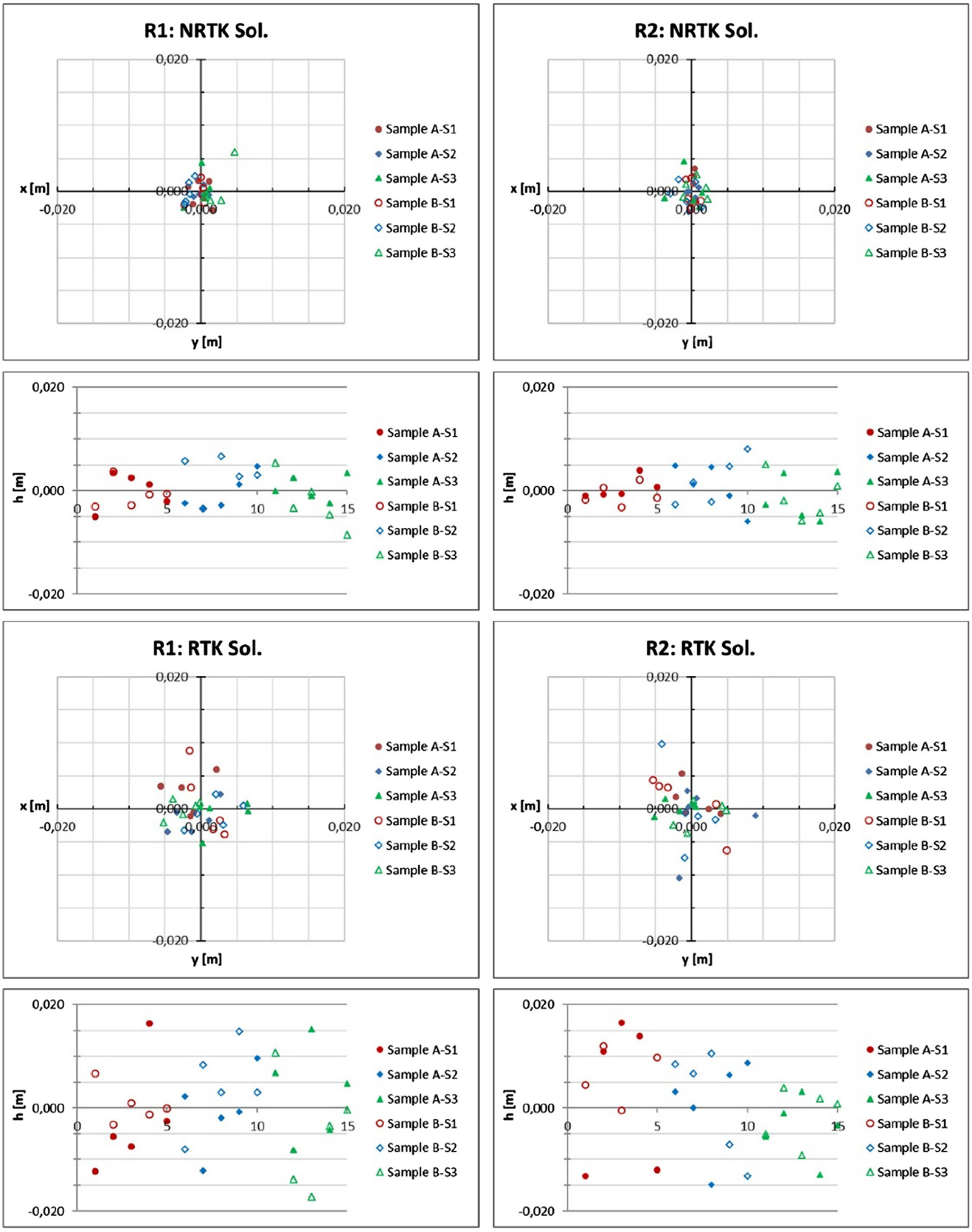

Fig. 5. Horizontal (northing and easting components) and vertical (h) residuals from NRTK (top) and single-base RTK (bottom) samples at rover points R1 and R2.

Table 1
Statistical results for the different samples in cases (a) and (b).

Statistical value	Case (a)		Case (b)	
	Sample A	Sample B	Sample A	Sample B
Mean value over the series of x_1 (m)	431501.6082	431501.6075	431501.6067	431501.6087
Mean value over the series of y_1 (m)	4182534.1433	4182534.1433	4182534.1476	4182534.1588
Mean value over the series of h_1 (m)	502.8191	502.8151	502.8203	502.8052
Mean value over the series of x_2 (m)	431511.6400	431511.6401	431511.6473	431511.6285
Mean value over the series of y_2 (m)	4182546.7240	4182546.7252	4182546.7245	4182546.7258
Mean value over the series of h_2 (m)	502.8017	502.8008	502.7905	502.7919
Summation of the squared residual for x (mm)	41	82	332	302
Summation of the squared residual for y (mm)	107	108	276	404
Summation of the squared residual for h (mm)	313	475	2624	2448
Degrees of freedom for X, Y, and h	28	28	28	28
Experimental standard deviation in x (mm)	±1.2	±1.7	±3.4	±3.3
Experimental standard deviation in y (mm)	±2.0	±2.0	±3.1	±3.8
Experimental standard deviation in h (mm)	±3.3	±4.1	±9.7	±9.3
Standard uncertainty of a single position (mm)	±1.6	±1.8	±3.3	±3.5
Standard uncertainty of a single height (mm)	±3.3	±4.1	±9.7	±9.3

Table 2
Full test procedure results (95% confidence level) for samples A and B in cases (a) and (b) (A: Null hypothesis accepted) (Units are mm).

Test	Null hypothesis	Alternative hypothesis	Case (a)				Case (b)			
	H_o	H_a	Sample A		Sample B		Sample A		Sample B	
1	$s_{xy} \leq \sigma_{xy}$	$s_{xy} > \sigma_{xy}$	$1.6 \leq 9.2$	A	$1.8 \leq 9.2$	A	$3.3 \leq 24.2$	A	$3.5 \leq 24.2$	A
2	$s_h \leq \sigma_h$	$s_h > \sigma_h$	$3.3 \leq 18.2$	A	$4.1 \leq 18.2$	A	$9.7 \leq 25.6$	A	$9.3 \leq 25.6$	A
3	$s_{xy(A)} = s_{xy(B)}$	$s_{xy(A)} \neq s_{xy(B)}$	$0.59 \leq 0.79 \leq 1.70$			A	$0.59 \leq 0.89 \leq 1.70$			A
4	$s_{h(A)} = s_{h(B)}$	$s_{h(A)} \neq s_{h(B)}$	$0.47 \leq 0.65 \leq 2.13$			A	$0.47 \leq 1.09 \leq 2.13$			A

Table 3
Combined standard uncertainty evaluation for the dual-frequency GNSS receiver Leica GS10 with AS10 antenna considering the NRTK solution.

Sources of uncertainty	Symbol	Evaluation	Distribution	Standard uncertainty Sample A	Standard uncertainty Sample B
I. Result of measurement					
Standard uncertainty of xy-coordinates	$u_{ISO\text{-}GNSS\text{-}xy}$	Type A	Normal	±1.6 mm	±1.8 mm
Standard uncertainty of h-coordinate	$u_{ISO\text{-}GNSS\text{-}h}$	Type A	Normal	±3.3 mm	±4.1 mm
II. Relevant sources of the GNSS receiver					
Sensitivity of the tubular level	u_{bub}	Type B	Specified by the manufacturer	0	0
Display round-off error	u_{disp}	Type B	Rectangular	±0.3 mm	±0.3 mm
III. Error pattern from the setting up of the instrument					
Centering	u_c	Type B	Normal	±1 mm	±1 mm
Antenna height	u_{ha}	Type B	Normal	±1 mm	±1 mm
Stability of a tripod height	u_{hs}	Type B	Rectangular	Neglectable	Neglectable
Antenna phase center offset parameter dx	u_{dx}	Type B	Normal	±1 mm	±1 mm
Antenna phase center offset parameter dy	u_{dy}	Type B	Normal	±1 mm	±1 mm
Antenna phase center offset parameter dh	u_{dh}	Type B	Normal	±2 mm	±2 mm
Multipath			Not considered		
Clock in the GNSS receiver or satellite			Not considered		
Orbit of the satellite			Not considered		
Ionospheric delay			Not considered		
Tropospheric delay			Not considered		
IV. Mathematical modeling					
Transformation	u_{tr}	Type A	Normal	Neglectable	Neglectable
Geoid undulation	u_{dH}	Type B	Rectangular	Neglectable	Neglectable
Combined uncertainty on the horizontal coordinates (mm)	u_{xy}			**±2.4**	**±2.5**
Combined uncertainty on the vertical coordinate (mm)	u_h			**±4.0**	**±4.7**
Expanded uncertainty on the horizontal coordinates (mm)	$U_{xy} = 2\ u_{xy}$			**±4.8**	**±5.0**
Expanded uncertainty on the vertical coordinate (mm)	$U_h = 2\ u_h$			**±8.0**	**±9.4**

to the error pattern for the setting up of the instrument, the uncertainty considered due to centering (u_c) and antenna height (u_{ha}) are different for both kinds of receivers. A tribrach with an optical plummet is used for setting up the instrument over the benchmarks allowing high accuracy in instrument centering. The considered standard uncertainty due to centering is set to ±1 mm for the dual-frequency receiver. In previous work, we could verify that this value can be reliable [43]. For the low-cost single-frequency receiver, the patch antenna is placed at the middle of a metallic ground plane (Fig. 2c) and thus, the standard uncertainty is set to ±3 mm. In relation to the antenna height, for the dual-frequency receiver, the height of the antenna above the benchmark consists of three components: the vertical phase center variations, the vertical offset, and the vertical height reading. Pre-configured standard

Table 4
Combined standard uncertainty evaluation for the low-cost single-frequency GNSS receiver u-blox NEO-M8P considering the single-base RTK solution.

Sources of uncertainty	Symbol	Evaluation	Distribution	Standard uncertainty Sample A	Standard uncertainty Sample B
I. Result of measurement					
Standard uncertainty of xy-coordinates	$u_{ISO\text{-}GNSS\text{-}xy}$	Type A	Normal	±3.3 mm	±3.5 mm
Standard uncertainty of h-coordinate	$u_{ISO\text{-}GNSS\text{-}h}$	Type A	Normal	±9.7 mm	±9.3 mm
II. Relevant sources of the GNSS receiver					
Sensitivity of the tubular level	u_{bub}	Type B	Specified by the manufacturer the manufacturer	0	0
Display round-off error	u_{disp}	Type B	Rectangular	±0.3 mm	±0.3 mm
III. Error pattern from the setting up of the instrument					
Centering	u_c	Type B	Normal	±3 mm	±3 mm
Antenna height	u_{ha}	Type B	Normal	±3 mm	±3 mm
Stability of a tripod height	u_{hs}	Type B	Rectangular	Neglectable	Neglectable
Antenna phase center offset parameter dx	u_{dx}	Type B	Normal	±2 mm	±2 mm
Antenna phase center offset parameter dy	u_{dy}	Type B	Normal	±2 mm	±2 mm
Antenna phase center offset parameter dh	u_{dh}	Type B	Normal	±4 mm	±4 mm
Multipath			Not considered		
Clock in the GNSS receiver or satellite			Not considered		
Orbit of the satellite			Not considered		
Ionospheric delay			Not considered		
Tropospheric delay			Not considered		
IV. Mathematical modeling					
Transformation	u_{tr}	Type A	Normal	Neglectable	Neglectable
Geoid undulation	u_{dH}	Type B	Rectangular	Neglectable	Neglectable
Combined uncertainty on the horizontal coordinates (mm)	u_{xy}			**±5.3**	**±5.4**
Combined uncertainty on the vertical coordinate (mm)	u_h			**±10.9**	**±10.6**
Expanded uncertainty on the horizontal coordinates (mm)	$U_{xy} = 2\ u_{xy}$			**±10.6**	**±10.8**
Expanded uncertainty on the vertical coordinate (mm)	$U_h = 2\ u_h$			**±21.8**	**±21.2**

settings in the instrument have been used, thus the receiver automatically considers the vertical phase center variations. As Leica standard antenna and accessories have been used, the vertical offset is known and is automatically taken into account. Finally, the vertical height reading is the height difference between the bottom end of the height hook and the benchmark. The standard uncertainty considered due to antenna height is set to ±1 mm. In the case of the single-frequency receiver, the uncertainty of antenna height is set to ±3 mm.

The combined standard and expanded uncertainties (probability of 95%) on the horizontal positions and heights, as determined according to Eqs. (6)–(9) respectively, are shown in Tables 3 and 4.

$$u_{xy} = \pm\sqrt{u^2_{ISO-GNSS-xy} + [h_a \tan(u_{bub})]^2 + 2u^2_{disp} + u^2_c + u^2_{dx} + u^2_{dy} + u^2_{tr}} \quad (6)$$

$$u_h = \pm\sqrt{u^2_{ISO-GNSS-h} + u^2_{disp} + u^2_{ha} + u^2_{hs} + u^2_{dh} + u^2_{dH}} \quad (7)$$

$$U_{xy} = 2u_{xy} \quad (8)$$

$$U_h = 2u_h \quad (9)$$

where h_a is the antenna height, u_{bub} is the sensitivity of the tubular/circular level, u_{disp} is the standard uncertainty of the minimum display digit $\left(0,5/\sqrt{3}\right)$, u_c is the centering standard uncertainty, u_{dx} and u_{dy} are the standard uncertainties antenna phase center offset parameters dx and dy, u_{tr} is the standard uncertainty in the transformation (mathematical modeling), u_{hs} is the standard uncertainty in the stability of the tripod height [44], u_{dh} is the standard uncertainty antenna phase center offset parameter dh, and u_{dH} is the standard uncertainty in the geoid undulation. Although antenna calibration is not available for low-cost antenna and taking into account their low-profile structure, we consider that the values of the standard uncertainties antenna phase center offset parameters dx and dy and the standard uncertainty antenna phase center offset parameter dh considered for the low-cost single frequency receiver could double the values generally considered for the dual-frequency GNSS receiver (Table 4).

For the dual-frequency receiver, the combined standard uncertainties on the horizontal position u_{xy} are in the order of ±2.5 mm and ±4–5 mm for the vertical components u_h. Slightly larger for the low-cost single-frequency receiver, the standard uncertainties for a single position u_{xy} are close to ±5.5 mm, and ±11 mm for height u_h. The results confirm that high precise positioning in real-time is guaranteed with Leica GS10 survey-grade dual-frequency receiver and demonstrate that precise positioning in real-time at centimeter level is also possible with the low-cost single-frequency u-blox NEO-M8P. However, it is important to keep in mind that the good results obtained by the low-cost receiver compared to the dual-frequency receiver used in this study may be due to the baseline length, at the order of 330 m. Further tests and analysis are required with longer baselines.

5. Conclusions

Dual-frequency GNSS receivers are widely used for many geomatic applications. However, low-cost single-frequency receivers have been relegated to navigation applications. Nevertheless, their main advantages (small size, ease of use, low-cost, and high precision positioning even in real-time) make them optimum candidates for positioning applications in many scientific areas including surveying, precision agriculture, and environmental or cadastral applications, among others. Because of this, this work evaluates the real-time positioning performance of a low-cost single-frequency receiver (u-blox NEO-M8P) using a single-base station solution and contrasts it with a geodetic dual-frequency one (Leica GS10 receiver with AS10 antenna) considering network-based solution. For that, the ISO standard 17123-8 for GNSS field measurement systems in RTK has been applied. As we expected, the tests results indicate that the geodetic receiver satisfies the horizontal and the vertical sub-centimetric precision limits

established for high precision applications, including network densification, topographic control, photogrammetric control points, even the evaluation of NRTK solutions. In addition, this study also demonstrates how a low-cost antenna combined with the single-frequency u-blox NEO-M8P receiver can be used to achieve centimeter-level precision in real-time, making it a low-cost choice for many surveying applications.

Considering the different sources of uncertainty and their influence quantities, the combined uncertainty budget for the dual-frequency receiver gives combined standard uncertainties on the horizontal position in the order of ±2.5 mm and close to ±4.5 mm for the vertical coordinate. In the case of the low-cost single-frequency receiver, the combined standard uncertainties are close to ±5.5 mm for the horizontal position and ±11 mm for heights. Although these values are slightly larger than for the dual-frequency receiver, as expected, the standard uncertainties are all below 1 cm. For both receivers, the horizontal uncertainty is approximately two times better than the vertical one. The excellent results achieved for the dual-frequency receiver should not hide that they may be affected by the NRTK correction (VRS, MAC...) used, the location of the rover points and their positions respect to the reference stations, the number of available satellites, their type (GPS, GLONASS, Galileo or a combination of them) and configuration (DOP), and the atmospheric conditions. Further tests are required in order to define correlation issues, especially in relation to the type of NRTK solution considered (VRS vs. MAC) or the distance to the nearest reference station.

As a final conclusion, it has been demonstrated that the low-cost GNSS receiver can achieve competitive positioning performance to survey-grade dual-frequency receivers in real-time positioning. This was shown empirically for short baselines (around 350 m) and specific instruments and conditions. However, subsequent analyses should be carried out for longer baselines.

Acknowledgements

This work was supported by the Center for Advanced Studies in Earth Sciences (Project: Analysis of erosion in olive groves using GNSS techniques), the RNM282 Research Group (Junta de Andalucía), and PAI UJA 2019/20 from the University of Jaén. Support provided by the Institute of Statistics and Cartography of Andalusia (RAP network) during this project is gratefully acknowledged. We also appreciate the support of Manuel Avilés and Sergio Blanca in leveling data collection. We thank the two anonymous reviewers, whose suggestions and corrections really helped to improve the paper.

References

[1] T. Takasu, A. Yasuda, Evaluation of RTK-GPS Performance with Low-cost Single-frequency GPS Receivers, in: Proc. 13th GPS/GNSS Symposium 2008, Nov. 11–14, Tokyo, Japan.
[2] R. Odolinski, P. Teunissen, Single-frequency, dual-GNSS versus dual-frequency, single-GNSS: a low-cost and high-grade receivers GPS-BDS RTK analysis, J. Geod. 90 (11) (2016) 1255–1278.
[3] R. Odolinski, P. Teunissen, Low-cost, high-precision, single-frequency GPS–BDS RTK Positioning, GPS Solutions 21 (2017) 1315–1330.
[4] R. Odolinski, P. Teunissen, An assessment of smartphone and low-cost multi-GNSS single-frequency RTK positioning for low, medium and high ionospheric disturbance periods, J. Geod. (2018), https://doi.org/10.1007/s00190-018-1192-5.
[5] M. Pepe, CORS architecture and evaluation of positioning by low-cost GNSS receiver, Geod. Cartography 44 (2) (2018) 36–44.
[6] P. Dabove, A.M. Manzino, GPS & GLONASS mass-market receivers: positioning performances and peculiarities, Sensors 14 (2) (2014) 22159–22179, https://doi.org/10.3390/s141222159.
[7] B. Wiśniewski, K. Bruniecki, M. Moszyński, Evaluation of RTKLIB's positioning accuracy using low-cost GNSS receiver and ASG-EUPOS, TransNav: International Journal on Marine Navigation and Safety of Sea Transportation 7 (1) (2013) 79–85, https://doi.org/10.12716/1001.07.01.10.
[8] L. Wanninger, Ionospheric Disturbance Indices for RTK and Network RTK Positioning, in: Proc. of ION GNSS 2004, Long Beach, CA.
[9] F. Takac, O. Zelzer. The Relationship Between Network RTK Solutions MAC, VRS, PRS, FKP and i-MAX, in: Proc. 21st International Technical Meeting of the Satellite Division of The Institute of Navigation (ION GNSS 2008), Savannah, GA, September 2008, 2008, pp. 348–355.
[10] H.J. Euler, C.R. Keenan, B.E. Zebhauser, G. Wübbena, Study of a simplified approach of utilizing information from permanent reference station arrays, in: Proc. 14th Int. Tech. Meeting Satellite Div. U.S. Inst. Navig., 2001, Salt Lake City, Utah.
[11] H. Landau, U. Vollath, X. Chen, Virtual reference station systems, J. Global Positioning Syst. 1 (2) (2002) 137–143.
[12] H.J. Euler, B.E. Zebhauser, The use of standardized network RTK messages in rover applications for surveying, in: Proc. of ION NTM 2003, January 22–24, Anaheim, CA.
[13] P.J.G. Teunissen, The least squares ambiguity decorrelation adjustment: a method for fast GPS integer estimation, J. Geod. 70 (1995) 65–82.
[14] V. Janssen, A Comparison of the VRS and MAC Principles for Network RTK, International Global Navigation Satellite Systems Society IGNSS Symposium, 2009, Australia.
[15] S.J. Edwards, P.J. Clarke, N.T. Penna, S. Goebell, An examination of network RTK GPS services in Great Britain, Survey Rev. 42 (316) (2010) 107–121.
[16] V. Janssen, J. Haasdyk, S. McElroy, D. Kinlyside, D. CORSnet-NSW: Improving Positioning Infrastructure for New South Wales, in: Proc. of Surveying & Spatial Sciences Institute Biennial International Conference (SSSC2011), Wellington, New Zealand.
[17] A. Martin, E. McGovern, An evaluation of the performance of network RTK GNSS services in Ireland, International Federation of Surveyors (FIG) Working Week, 6th–10th May 2012. Rome, Italy.
[18] T.K. Yeh, B.F. Chao, C.S. Chen, C.H. Chen, Z.Y. Lee, Performance improvement of network based RTK GPS positioning in Taiwan, Survey Rev. 44 (2012) 3–8.
[19] M.S. Garrido, E. Giménez, M.C. De Lacy, A.J. Gil, Dense regional active networks and high accuracy positioning services. A case study based on the andalusian positioning network (southern Spain), IEEE J. Sel. Top. Appl. Earth Obs. Remote Sens. 6 (2013) 2421–2433.
[20] K. Gumus, M.O. Selbesoglu, C.T. Celik, Accuracy investigation of height obtained from Classical and Network RTK with ANOVA test, Measurement 90 (2016) 135–143.
[21] ISO, International Standard ISO 17123-8: 2007 – Optics and optical instruments – Field procedures for testing geodetic and surveying instruments – Part 8: GNSS field measurement systems in real-time kinematic (RTK)", ISO, Geneva, Switzerland. International Standardization Organization, 2007.
[22] ISO, "International Standard ISO 17123-8: 2015 – Optics and optical instruments – Field procedures for testing geodetic and surveying instruments – Part 8: GNSS field measurement systems in real-time kinematic (RTK)", ISO, Geneva, Switzerland. International Standardization Organization, 2015.
[23] H. Heister, The new ISO standard 17123-8 for checking GNSS field measuring systems, FIG Working Week 2008, Stockholm, Sweden, 14–19 June 2008.
[24] A. Sioulis, M. Tsakiri, D. Stathas, Evaluation of low cost, high sensitivity GNSS receivers based on the ISO RTK standards, Int. J. Geomatics Geosci. 6 (2) (2015) 1597–1606.
[25] M. Tsakiri, A. Sioulis, G. Piniotis, Compliance of low-cost, single-frequency GNSS receivers to standards consistent with ISO for control surveying, Int. J. Metrol. Qual. Eng. 8 (11) (2017) 1–12.
[26] E. Lambrou, N. Kanellopoulos, Check and calibration of a single GNSS receiver by using the VRS RTN positioning method, Measurement 117 (2018) 221–225.
[27] M.C. De Lacy, F. Sansò, G. Rodriguez-Caderot, A.J. Gil, The Bayesian approach applied to GPS ambiguity resolution. A mixture model for the discrete-real ambiguities alternative, J. Geod. 76 (2002) 82–94.
[28] M. Crespi, A software package for the adjustment and the analysis of GPS control networks, in: M. Unguendoli (Ed.), In reports on Survey and Geodesy in memory of Prof. A. Gubellini and G. Folloni, Edizioni Nautilus, Bologna, 1996.
[29] RTCM Recommended Standards for Differential GNSS (Global Navigation Satellite Systems) Service, Version 3.0, RTCM Paper 30-2004/SC104-STD. 2004.
[30] Leica Geosystems, Leica Viva Series Technical Reference Manual, 2014, 934 pp.
[31] u-blox, Achieving centimeter level performance with low cost antennas, White paper. Document no. UBX-16010559-R01, 2018 (www.u-blox.com. Last accessed: July 10, 2018).
[32] u-blox AG, UBX-15015836 – R07. Production Information. 2017.
[33] RAP, 2018 (http://www.ideandalucia.es/portal/web/portal-posicionamiento/rap. Last accessed: 11 June 2018).
[34] R. Páez, C. Torrecillas, I. Barbero, M. Berrocoso, Regional positioning services as economic and construction activity indicators: the case study of Andalusian Positioning Network (Southern Spain), Geocarto Int. 32 (1) (2017) 44–58.
[35] National Geographic Institute (Instituto Geográfico Nacional), Normas para la nivelación geométrica de alta precisión con equipos digitales, 2014. (ftp://ftp.geodesia.ign.es/REDNAP/Documentacion. Last accessed: July 10, 2018).
[36] ISO, International Standard ISO 17123-2: 2001. Optics and optical instruments – Field procedures for testing geodetic and surveying instruments – Part 2: Levels, Geneva, Switzerland, International Standardization Organization, 2001.
[37] L. Biagi, F. C. Grec, A. Fermi, M. Negretti. Relative antenna calibration for mass-market GNSS receivers: A case study, 2018 (Unpublished). https://doi.org/10.13140/rg.2.2.19687.09123.

[38] C.R. Greenwalt, M.C. Shultz, Principles of error theory and cartographic applications, ACIC Technical Report No. 96, St. Louis, Missouri, Aeronautical Chart and Information Center, USAF, 1962.
[39] G.W. Corder, D.I. Foreman, Nonparametric Statistics: A Step-by-Step Approach ISBN 978-1118840313, Wiley, New York, 2014.
[40] E.L. Lehmann, Fisher, Neyman, and the Creation of Classical Statistics, Springer, 2011.
[41] A.M. Ruiz-Armenteros, J.L. García-Balboa, J.L. Mesa-Mingorance, J.J. Ruiz-Lendínez, M.I. Ramos-Galán, Contribution of instrument centring to the uncertainty of a horizontal angle, Survey Rev. 45 (331) (2013) 305–314.
[42] J.L. García-Balboa, A.M. Ruiz-Armenteros, J.L. Mesa-Mingorance, Evaluación de la incertidumbre de medida de ángulos, distancias y desniveles medidos con instrumentación topográfica, Mapping 149 (2011) 6–27 (in Spanish).
[43] J.L. García-Balboa, A.M. Ruiz-Armenteros, J. Rodríguez-Avi, J.F. Reinoso-Gordo, J. Robledillo-Román, A field procedure for the assessment of the centring uncertainty of geodetic and surveying instruments, Sensors 18 (10) (2018) 3187.
[44] ISO, International Standard ISO 12858-2: 1999. Optics and optical instruments — Ancillary devices for geodetic instruments — Part 2: Tripods. Geneva, Switzerland, International Standardization Organization, 1999.